Applied Physics Letters ARTICLE scitation.org/journal/apl

Efficient scattering-free wavefront transformation with power flow conformal bianisotropic acoustic metasurfaces

Cite as: Appl. Phys. Lett. **118**, 061902 (2021); doi: 10.1063/5.0033422
Submitted: 2 November 2020 · Accepted: 14 January 2021 ·
Published Online: 11 February 2021

Xiuyuan Peng, Junfei Li, Chen Shen, and Steven A. Cummer[a)]

AFFILIATIONS

Department of Electrical and Computer Engineering, Duke University, Durham, North Carolina 27708, USA

[a)]Author to whom correspondence should be addressed: cummer@duke.edu

ABSTRACT

Bianisotropic metasurfaces have enabled highly efficient wavefront transformation. However, a passive and lossless bianisotropic metasurface must conserve local power at every point over the metasurface, hindering its application in handling complicated wavefields other than plane waves. In this paper, the power flow-conformal design methodology and bianisotropic unit cells are combined to comply with such a restriction. Our proposed approach provides a general recipe for arbitrary wavefront transformation with maximum power efficiency. As a demonstration, a transmission-type acoustic metasurface was designed to focus 3000 Hz plane wave airborne sound in the near field with theoretically unitary power efficiency. The metasurface was validated by both numerical simulation and experiment.

People have long been interested in shaping sound waves. Conventional beam-forming techniques require active transducers with phase control circuits, which are costly and complicated. Recently, passive acoustic metasurfaces have been used to reshape acoustic waves in a variety of ways.[1–4] The simplest acoustic metasurfaces are designed based on the generalized Snell's law[5–8] and rely on a linear transmission phase gradient along the metasurface.

However, linear phase gradient metasurfaces (LPGMs) unavoidably generate multiple diffractive orders that are generally undesirable. These higher order modes not only distort the transmitted sound field but also reduce the energy transmission efficiency since the acoustic power is carried by these unwanted modes. Improvements were made by using arbitrary phase modulation along the metasurface to match the field distribution on both sides.[9] Later, amplitude modulation was incorporated into the unit cells to further suppress parasitic diffraction.[10,11] This method comes with a price that in order to achieve amplitude modulation, the unit cells must be lossy so that the overall power transmission efficiency is reduced. As a result, a question was raised that we can design a "perfect" metasurface that simultaneously suppresses unwanted modes and maximizes efficiency.

For reflection-type metasurfaces, one path toward a perfect metasurface is to design nonlocal coupling of sound waves along the metasurface,[12] but this metasurface is hard to realize experimentally. Another way is to employ a curved, power flow-conformal design[13] where the intensity flow of the total sound field is, by design, tangential to the metasurface interface. By complying with the requirement of local power conservation, the total power efficiency of this metasurface is maximized.

For transmission-type metasurfaces, it has been shown that scattering-free manipulation of sound can be achieved by using bianisotropic unit cells.[14–17] The advantages of using bianisotropic unit cells are that they can be theoretically passive while achieving higher-than-unity pressure transmission coefficients.[18,19] This enables manipulation of sound waves without scattering into unwanted modes. However, passive and lossless bianisotropic unit cells require the power flow on both sides of the metasurface to be balanced locally, which is not true for the most general wavefront transformation. While bianisotropic metasurface design works well with incident and transmitted plane waves, it cannot be used by itself to realize more complex wave patterns like focusing or beam splitting for which normal power is not conserved.[20] In these cases, a maximally efficient wavefront transformation requires either gain media or local energy redistribution along the metasurface.[21] To solve the power disparity problem with bianisotropic metasurfaces, people have augmented them with auxiliary surface waves[20,22] or implemented double-layer structures.[23] Nevertheless, these two designs suffer from disadvantages such as low conversion efficiency between propagating and surface modes and bulky geometries, respectively.

Here, we show that we can combine the merits of bianisotropic metasurfaces and power flow-conformal metasurfaces to achieve highly efficient manipulation of arbitrary acoustic wavefronts. The optimal geometric profile of the metasurface is determined by matching the normal components of the incident and transmitted sound intensity fields so that the power flow is balanced locally. Then, the local pressure field transformation is realized using bianisotropic unit cells. As a demonstration, we designed a power-flow conformal bianisotropic metasurface (PFCBM) that focuses a planar incident wave in the near field and verified the design with simulation and experiments.

We start with the general case where the incident sound pressure field p_i is transformed to the transmitted field p_t. For simplicity, we consider time-harmonic waves in the 2D scenario so that $p_i = p_i(\vec{r})e^{j\omega t}$ and $p_t = p_t(\vec{r})e^{j\omega t}$, where $\vec{r} = x \cdot \hat{x} + z \cdot \hat{z}$ and ω is the angular frequency of the sound. We would drop the time-harmonic term $e^{j\omega t}$ in the following derivations for conciseness. Using the acoustic wave equation in 2D: $\rho \frac{\partial \vec{v}}{\partial t} + \nabla p = 0$, where $\nabla p = \frac{\partial p}{\partial x} + \frac{\partial p}{\partial z}$, the particle velocity of both the incident and transmitted sound fields can be written as $\vec{v} = \hat{x} \cdot v_x + \hat{z} \cdot v_z$. Once the required sound pressure field and particle velocity field are known, the corresponding sound intensity field can be calculated by $\vec{I} = \frac{1}{2}\mathrm{Re}(p \cdot \vec{v}^*)$.

We then find the optimal geometric shape of the metasurface to ensure that the metasurface is power flow-conformal. We assume an infinitely thin acoustic metasurface located at $z_s = z_s(x)$. If the normal component of the incident sound intensity vector and the normal component of the transmitted sound intensity vector are not the same on both sides of the metasurface, i.e., $\vec{I}_i(x, z_s) \cdot \hat{n}(x, z_s) \neq \vec{I}_t(x, z_s) \cdot \hat{n}(x, z_s)$, then there must be net acoustic energy absorbed or generated within the metasurface locally, corresponding to loss or gain of the metasurface material. One way to achieve 100% energy transmittance is to distribute the loss and gain so that they average to zero along the metasurface.[24] However, this method is not practically plausible as there lack passive gain acoustic materials to facilitate such loss/gain pattern.

Here, we adopt another strategy: the geometric shape of the metasurface is tuned so that the metasurface is power flow-conformal, i.e., $\vec{I}_i(x, z_s) \cdot \hat{n}(x, z_s) = \vec{I}_t(x, z_s) \cdot \hat{n}(x, z_s)$. In this way, the required metasurface can be lossless and passive. We define the residual sound intensity field as

$$\Delta\vec{I} = \vec{I}_t - \vec{I}_i = \hat{x} \cdot \Delta I_x + \hat{z} \cdot \Delta I_z. \tag{1}$$

Thus, the problem becomes how to find a curve such that the $\Delta\vec{I}$ field normal to the curve is always zero. We also define an auxiliary vector field $\vec{N} = -\hat{x} \cdot \Delta I_z + \hat{z} \cdot \Delta I_x$. It can be proven that[13] if the fields on both sides of the metasurface are source-free, i.e., $\nabla \cdot I_1 = \nabla \cdot I_2 = 0$, then we have $\nabla \times \vec{N} = 0$ so that $\vec{N}$ can be written as the gradient of a scalar field, $\nabla g = -\vec{N}$.

It can be seen that $\vec{N}$ is perpendicular to $\Delta\vec{I}$. Suppose $z_g = z_g(x)$ is one of the level curves of the scalar potential function g ($g[x, z_g(x)]$ = Const.), then the normal vector along z_g must be parallel to the $\vec{N}$ vector, i.e., $\vec{N}(x, z_g) // \hat{n}(x, z_g)$. As a result, the power flow-conformal condition $\Delta\vec{I}(x, z_g) \cdot \hat{n}(x, z_g) = 0$ is satisfied. In short, the geometric profile of the metasurface should be chosen from the set of z_g, i.e., $z_s \in \{z_{g1}, z_{g2}, z_{g3}, \ldots\}$. After choosing one specific $z_s = z_g|_{z_g(0)=z_0}$, both the incident field and the transmitted field are determined everywhere on the x–z plane.

Third, we derive the physical structure of the proposed metasurface with the field distribution on both sides. The local response of the acoustic metasurface can be characterized by a 2×2 surface impedance matrix $Z = Z(x, z_s)$, whose elements Z_{11}, Z_{12}, Z_{21}, and Z_{22} are defined by

$$\begin{bmatrix} p_i(x, z_s) \\ p_t(x, z_s) \end{bmatrix} = \begin{bmatrix} Z_{11} & Z_{12} \\ Z_{21} & Z_{22} \end{bmatrix} \cdot \begin{bmatrix} \hat{n}(x, z_s) \cdot \vec{v}_i(x, z_s) \\ \hat{n}(x, z_s) \cdot -\vec{v}_t(x, z_s) \end{bmatrix}. \tag{2}$$

Since the metasurface is lossless and passive, the impedance matrix is purely imaginary, i.e., $Z_{mn} = jX_{mn}$. We can then re-write the impedance matrix in the following form so that each element can be determined with the field distribution:

$$\begin{bmatrix} \mathrm{Re}(p_i) & \mathrm{Im}(p_i) \\ \mathrm{Re}(p_t) & \mathrm{Im}(p_t) \end{bmatrix} = \begin{bmatrix} X_{11} & X_{12} \\ X_{21} & X_{22} \end{bmatrix} \cdot \begin{bmatrix} -\mathrm{Im}(\hat{n} \cdot \vec{v}_i) & \mathrm{Re}(\hat{n} \cdot \vec{v}_i) \\ \mathrm{Im}(\hat{n} \cdot \vec{v}_t) & -\mathrm{Re}(\hat{n} \cdot \vec{v}_t) \end{bmatrix}. \tag{3}$$

After the surface impedance profile is determined, we then discretize the metasurface into a finite number of bianisotropic unit cells. Here, we choose to use a hybrid structure composed of shunted Helmholtz resonators and a straight channel, as shown in Fig. 2(a). The depths of the cavities w_a, w_b, w_c w_d as well as the channel width w_1 can be varied to achieve the required bianisotropic response. The details of the geometry are explained in the supplementary material. It has been shown in Refs. 14 and 15 that such design possesses a large degree of freedom and ensures compact structures.

As an example, a power flow-conformal bianisotropic metasurface (PFCBM) is designed for sound focusing. As shown in Fig. 1(a), plane incident sound $p_i = A_i \exp(-jkz)$ is focused to a single point at (0, 0) after transmitting through the metasurface. The transmitted sound can be written as $p_t = A_t H_0^{(1)}(kr)$ accordingly, where $H_0^{(1)}(x)$ is the zeroth order Hankel function of the first kind. Here, $k = \omega/c$ is the wavenumber in air. $f = 3000$ Hz is the designed frequency. $c = 343$ m/s is the sound speed in air. A_i and A_t are the amplitudes of the incident and transmitted waves, respectively. The particle velocity fields of the incident and transmitted waves are

$$\begin{cases} v_{x,i} = 0, \\ v_{z,i} = A_i \exp(-jkz)/Z_0 \end{cases} \tag{4}$$

and

$$\begin{cases} v_{x,t} = -jA_t H_1^{(1)}(kr)\dfrac{x}{Z_0 r}, \\ v_{z,t} = -jA_t H_1^{(1)}(kr)\dfrac{z}{Z_0 r}. \end{cases} \tag{5}$$

Here, $Z_0 = \rho c$ is the characteristic acoustic impedance of the air, and $\rho = 1.225\,\mathrm{kg/m^3}$ is the density of the air at room temperature. $H_1^{(1)}(x)$ is the first order Hankel function of the first kind. Without losing generality, we assume $A_i = 1$. Once the focal length $f = -z_0$ is decided, we can calculate A_t by equating the values of sound intensity along the z direction at $(0, z_0)$. Then, we simply write the g field and find the level curve that crosses $(0, z_0)$. Following the methodology, as mentioned before, the PFCBM can be designed. The scalar potential field $g(x, z)$ and the metasurface geometry $z_s = z_s(x)$ are shown in Fig. 1(b). It suggests an important divergence from the plane wave

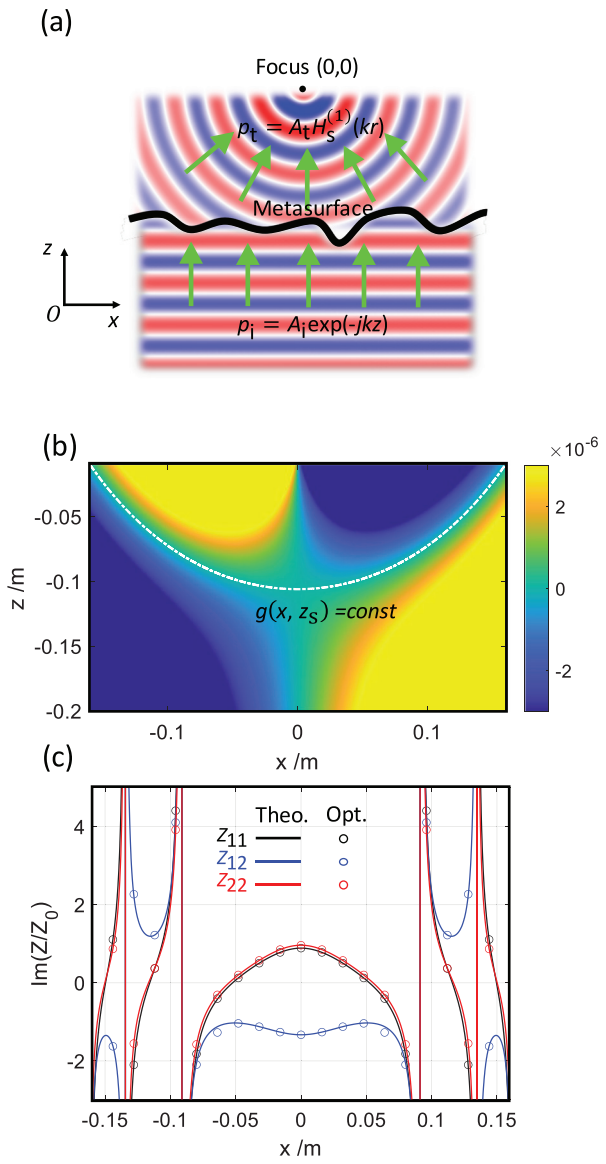

FIG. 1. (a) Schematic of the power flow-conformal bianisotropic metasurface (PFCBM). (b) The scalar potential field $g(x, z)$ and the geometry of the proposed sound focusing metasurface. (c) Impedance profile along the proposed metasurface. Theo.: theory. Opt.: optimization.

reflection design, as mentioned in Ref. 13. We also mention here that the shape of the metasurface is different from the trivial guess of a circle, hyperbolic curve, or a parabola. The geometric shape of the PFCBM for single-point focusing is governed by a Riccati equation, which can be found in the supplementary material.

The metasurface is then discretized into 19 unit cells spanning an aperture of 0.31 m. The corresponding impedance of each unit cell is shown in Fig. 1(c). The curves represent the theoretical calculation, while the circles represent optimized unit cells. The difference in Z_{11} and Z_{22} indicates that our design is bianisotropic.[25] The focal length is $f = 0.106$ m. In order to find the optimal geometric parameters for the

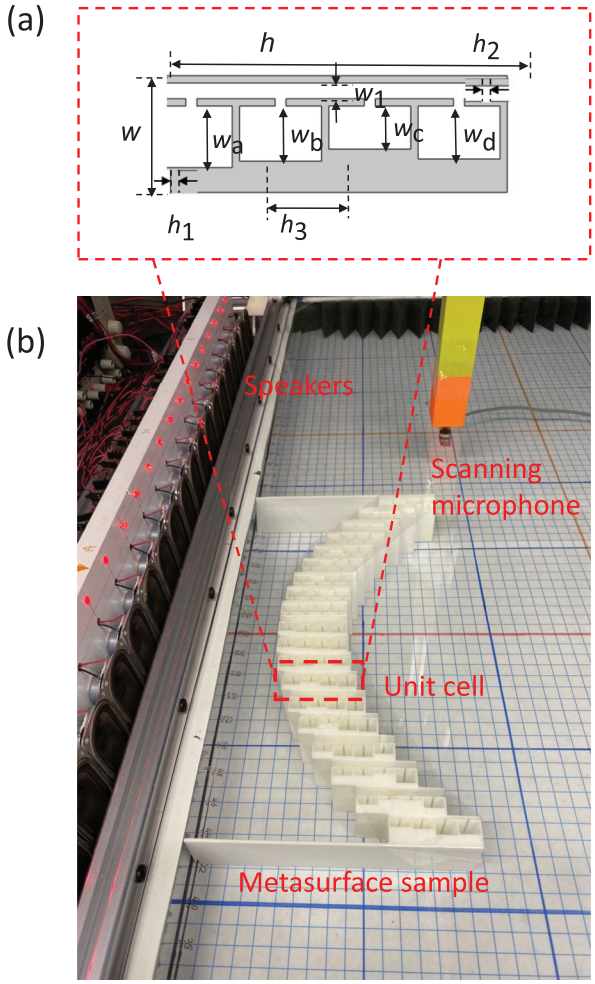

FIG. 2. (a) The geometry of the unit cell. (b) Experimental setup.

bianisotropic unit cells, we first run the genetic algorithm to derive the approximate values of all the parameters with randomized initial population and then use the pattern search algorithm to find the exact value of each parameter. In genetic algorithm optimization, the impedance matrix of the structure is calculated analytically for computational efficiency, while in pattern search, the impedance matrix of a structure is retrieved in COMSOL simulations for accuracy. The method for analytical calculation and parameter retrieval in simulations are outlined in Ref. 14. For simplicity, only the depths of the cavities of the four Helmholtz resonators w_a, w_b, w_c, w_d and the channel width w_1 are optimized for, while other geometric parameters are fixed for all unit cells. The details of the geometric parameters of our design can be found in the supplementary material.

We use the Pressure Acoustic module in COMSOL Multiphysics 5.4 to perform a numerical simulation with our PFCBM design. The sound intensity amplitude $|\vec{I}|$ is shown in Fig. 3(c) in arbitrary units. For comparison, we have also drawn the sound intensity map of a linear phase gradient metasurface (LPGM) in Fig. 3(a) and the sound intensity map of an arbitrary phase modulation metasurface (APMM)

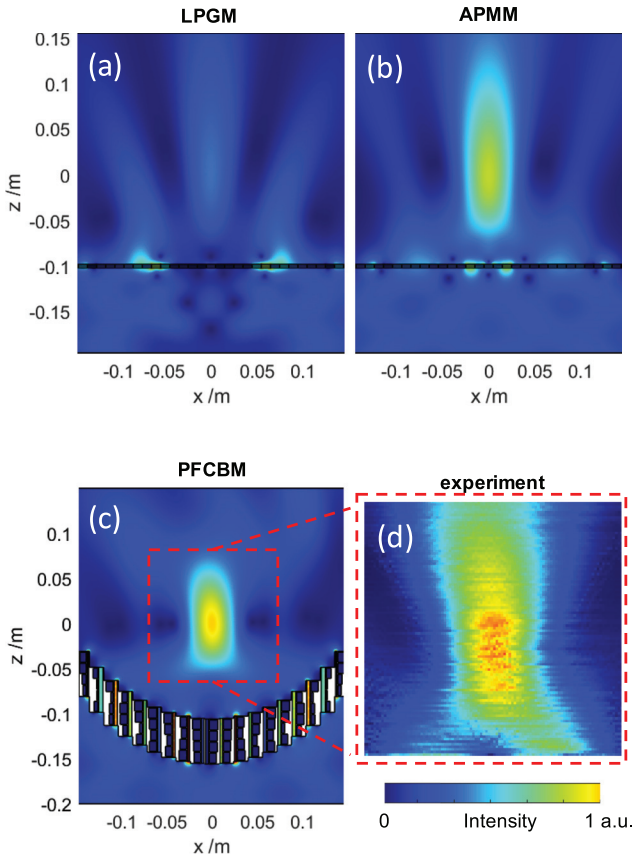

FIG. 3. Sound intensity map of the metasurfaces under plane wave incidence. Colors are in arbitrary units. (a) Linear phase gradient metasurface (LPGM). (b) Arbitrary phase modulation metasurface (APMM) designed with the synthetic field distribution. (c) Power-flow conformal bianisotropic metasurface (PFCBM). (d) PFCBM, experimental result.

designed with the synthetic field distribution method[9] in Fig. 3(b). We can find that our PFCBM can better localize the sound intensity around the focal point (0, 0) compared with the other two metasurface designs. Also, as is shown in Figs. 4(a) and 4(b), the PFCBM has higher power transmittance than the other two designs. We calculate the power transmittance of all three metasurfaces by integrating the sound intensity amplitudes along the x axis. Both the large region ($x \in [-0.15, 0.15]$ m) and the small region ($x \in [-0.05, 0.05]$ m) results are shown in Table I.

For the experiments, we fabricated the designed metasurface with 3D printing and measured its performance in a 2D waveguide. The experimental setup is shown in Fig. 2(b). A line array of loudspeakers served as the sound source. To generate an incident plane wave, all speakers were calibrated so that their output sound pressure amplitudes and phases were the same. A microphone scanned across the region of interest to image the 2D sound field with a step size of 5 mm. Sound absorbing foam was placed around the edges to prevent echoes. We sent a Gaussian pulse centered at 3000 Hz to drive the speakers and time-gate the measured signal to minimize reflection from the boundaries. Fourier transform was used to extract the sound pressure signal's amplitude and phase at 3000 Hz from the measured acoustic

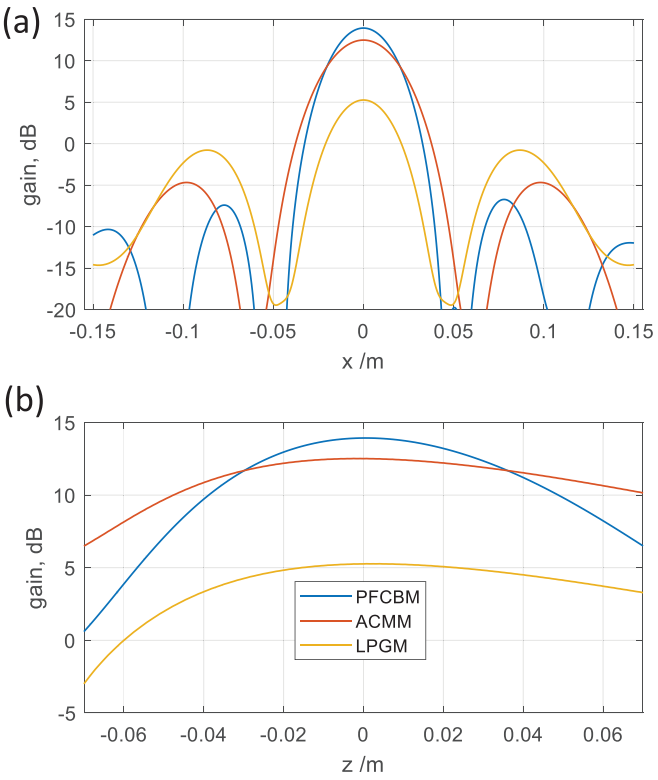

FIG. 4. (a) Sound intensity gain along $z = 0$. (b) Sound intensity gain along $x = 0$. All curves are compared with the incident sound intensity. We can see that the sound transmitted through the power flow-conformal bianisotropic metasurface (PFCBM) has higher energy as well as is better localized.

waveforms. Then, we calculate the particle velocity field $\vec{v}$ by implementing numerical spatial gradient on the sound pressure data. After that, the sound intensity $\vec{I} = \frac{1}{2}\mathrm{Re}[p^*\vec{v}]$ could be readily derived. The experimental results are shown in Fig. 3(d). It can be seen that the acoustic energy is focused at the desired location as designed, and diffraction into unwanted modes is suppressed compared to the other two approaches shown in Fig. 4. It is worth noting that although our design is 100% efficient in theory, factors such as finite unit cell discretization, fabrication errors, and thermoviscous loss prevent it from achieving 100% efficiency in practice.

To conclude, we have shown that a highly efficient metasurface for arbitrary wavefront transformation can be constructed by combining a power flow-conformal geometric profile with bianisotropic unit cells. This design is purely passive and can direct 100% of the transmitted energy to the desired focal point in theory. Moreover, the design

TABLE I. Energy transmittance.

Metasurface type	$(-0.15, 0.15)$ m	$(-0.05, 0.05)$ m
LPGM	60.8%	27.8%
APMM	95.4%	76.0%
PFCBM	97.4%	85.0%

process is general and applies to arbitrary wavefront manipulation scenarios as long as the incident and transmitted sound fields can be specified precisely. This work has potential applications in sensing, ultrasound therapy, nondestructive testing, and other fields where efficient sound focusing is of interest. The proposed framework for arbitrary wavefront manipulation is also expected to work for electromagnetic metasurfaces.

AUTHORS' CONTRIBUTIONS

X.P. and J.L. contributed equally to this paper.

See the supplementary material for the geometrical parameters of the unit cells of the PFCBM and detailed discussion of the geometric shape of the PFCBM.

This work was supported by an Emerging Frontiers in Research and Innovation grant from the National Science Foundation (Grant No. 1641084) and a CMMI grant from the National Science Foundation (Grant No. 1951106). The authors would like to thank Ailing Song and Xiaohui Zhu for their useful discussion.

DATA AVAILABILITY

The data that support the findings of this study are available from the corresponding author upon reasonable request.

REFERENCES

[1]Y. Li, X. Jiang, R.-Q. Li, B. Liang, X.-Y. Zou, L.-L. Yin, and J.-C. Cheng, Phys. Rev. Appl. **2**, 064002 (2014).
[2]J. Chen, J. Xiao, D. Lisevych, A. Shakouri, and Z. Fan, Nat. Commun. **9**, 4920 (2018).
[3]T. Liu, X. Zhu, F. Chen, S. Liang, and J. Zhu, Phys. Rev. Lett. **120**, 124502 (2018).
[4]R. Al Jahdali and Y. Wu, Appl. Phys. Lett. **108**, 031902 (2016).
[5]N. Yu, P. Genevet, M. A. Kats, F. Aieta, J.-P. Tetienne, F. Capasso, and Z. Gaburro, Science **334**, 333 (2011).
[6]Y. Xie, W. Wang, H. Chen, A. Konneker, B.-I. Popa, and S. A. Cummer, Nat. Commun. **5**, 5553 (2014).
[7]Y. Li, B. Liang, X. Tao, X.-F. Zhu, X.-Y. Zou, and J.-C. Cheng, Appl. Phys. Lett. **101**, 233508 (2012).
[8]W. Wang, Y. Xie, A. Konneker, B.-I. Popa, and S. A. Cummer, Appl. Phys. Lett. **105**, 101904 (2014).
[9]N. M. Estakhri and A. Alù, Phys. Rev. X **6**, 041008 (2016).
[10]Y. Zhu, J. Hu, X. Fan, J. Yang, B. Liang, X. Zhu, and J. Cheng, Nat. Commun. **9**, 1632 (2018).
[11]Y. Fang, X. Zhang, and J. Zhou, Appl. Phys. Lett. **110**, 171904 (2017).
[12]L. Quan and A. Alù, Phys. Rev. Appl. **11**, 054077 (2019).
[13]A. Díaz-Rubio, J. Li, C. Shen, S. A. Cummer, and S. A. Tretyakov, Sci. Adv. **5**, eaau7288 (2019).
[14]J. Li, C. Shen, A. Díaz-Rubio, S. A. Tretyakov, and S. A. Cummer, Nat. Commun. **9**, 1342 (2018).
[15]J. Li, A. Díaz-Rubio, C. Shen, Z. Jia, S. Tretyakov, and S. Cummer, Phys. Rev. Appl. **11**, 024016 (2019).
[16]L. Quan, Y. Ra'di, D. L. Sounas, and A. Alù, Phys. Rev. Lett. **120**, 254301 (2018).
[17]A. Melnikov, Y. K. Chiang, L. Quan, S. Oberst, A. Alù, S. Marburg, and D. Powell, Nat. Commun. **10**(1), 3148 (2019).
[18]V. S. Asadchy, M. Albooyeh, S. N. Tcvetkova, A. Díaz-Rubio, Y. Ra'di, and S. Tretyakov, Phys. Rev. B **94**, 075142 (2016).
[19]A. Díaz-Rubio and S. A. Tretyakov, Phys. Rev. B **96**, 125409 (2017).
[20]J. Li, A. Song, and S. A. Cummer, Phys. Rev. Appl. **14**, 044012 (2020).
[21]Z. Hou, X. Fang, Y. Li, and B. Assouar, Phys. Rev. Appl. **12**, 034021 (2019).
[22]A. Epstein and G. V. Eleftheriades, Phys. Rev. Lett. **117**, 256103 (2016).
[23]V. G. Ataloglou, A. H. Dorrah, and G. V. Eleftheriades, IEEE Trans. Antennas Propag. **68**, 7382 (2020).
[24]D. L. Sounas, R. Fleury, and A. Alù, Phys. Rev. Appl. **4**, 014005 (2015).
[25]M. B. Muhlestein, C. F. Sieck, P. S. Wilson, and M. R. Haberman, Nat. Commun. **8**(1), 15625 (2017).